

## Electromagnetothermoelastic behavior of a rotating imperfect hybrid functionally graded hollow cylinder

M. Saadatfar<sup>a</sup> and M. Aghaie-Khafri\*

Faculty of Mechanical Engineering, K.N. Toosi University of Technology, Postal Code: 1999143344,  
Tehran, Iran

(Received September 2, 2013, Revised February 20, 2014, Accepted February 24, 2014)

**Abstract.** The electro-magneto-thermo-elastic behavior of a rotating functionally graded long hollow cylinder with functionally graded piezoelectric (FGPM) layers is analytically analyzed. The layers are imperfectly bonded to its inner and outer surfaces. The hybrid cylinder is placed in a constant magnetic field subjected to a thermo-electro-mechanical loading and could be rested on a Winkler-type elastic foundation. The material properties of the FGM cylinder and radially polarized FGPM layers are assumed to be graded in the radial direction according to the power law. The hybrid cylinder is rotating about its axis at a constant angular velocity. The governing equations are solved analytically and then stresses, displacement and electric potential distribution are calculated. Numerical examples are given to illustrate the effects of material in-homogeneity, magnetic field, elastic foundation, applied voltage, imperfect interface and thermo-mechanical boundary condition on the static behavior of a FG smart cylinder.

**Keywords:** functionally graded piezoelectric (FGPM); functionally graded material (FGM); magnetic field; Imperfect bonding; elastic foundation

### 1. Introduction

Recently, material structures consisting of piezoelectric components have been intensively investigated due to their potential for converting one form of energy to one another. They have found increasing applications in intelligent structures as actuators and sensors. Functionally graded piezoelectric material (FGPM) is a kind of piezoelectric material with material composition and properties varying continuously along certain directions. FGPM is a composite material that is intentionally designed to possess desirable properties for some specific applications. FGM is made of a mixture with arbitrary composition of two different materials. The volume fraction of each material changes continuously and gradually. FGM is attractive due to its many engineering applications in magnetic storage elements, plasma physics and the corresponding measurement techniques of magneto-thermo-elasticity. Stresses in FGM structures under mechanical or thermal loads can be optimized by selecting proper material distribution.

It is possible to make intelligent hybrid materials by combining piezoelectric materials with

---

\*Corresponding author, Associate Professor, E-mail: [maghaei@kntu.ac.ir](mailto:maghaei@kntu.ac.ir)

<sup>a</sup> Ph.D. Student, E-mail: [msaadatfar@dena.kntu.ac.ir](mailto:msaadatfar@dena.kntu.ac.ir)

structural materials. New structures including FGM members bonded with piezoelectric actuators and sensors are smart in response to environmental changes. So, the integration of piezoelectric materials and composite materials or FGMs has become an attractive subject in the area of smart material and structures. Static analysis of functionally graded hollow cylinder with piezoelectric layers with different boundary condition was studied by Alibeigloo (2009, 2010). The functionally graded hollow thick cylinder with a piezoelectric ring is analyzed using FEM by Yas *et al.* (2011). Javanbakht *et al.* (2009) analyzed dynamic behavior of functionally graded shell with piezoelectric layers based on elasticity. The transient responses in a two-layered elasto-piezoelectric composite hollow cylinder in the state of axisymmetric plane strain are obtained by Wang (2007). Shakeri *et al.* (2009) studied dynamic response of functionally graded plate integrated with two piezoelectric layers, based on elasticity solution. Shen and Noda (2007) presented post-buckling analysis of a FGM cylindrical shell with piezoelectric actuators. Alibeigloo (2011) provided a thermo-elastic solution for axisymmetric deformations of a functionally graded cylindrical shell bonded to thin piezoelectric layers. To the best of authors' knowledge using the piezoelectric layers as sensor and actuator in hybrid cylinder is considered in many papers. But, the application of FGPM layers as sensor and actuator in hybrid cylinder is rarely studied. Recently, the thermo-electro-elastic analytical solution of a long functionally graded hollow cylinder bonded to functionally graded piezoelectric layers was presented by authors (Aghaie khafri and Saadatfar 2013).

Rotating disks and cylinders have important applications in rotating machinery and structures. The stress analysis of rotating homogeneous isotropic, orthotropic and anisotropic disks and cylinders has been an important topic in engineering design and applications (Chang 1975, Genta and Gola 1981, Tutuncu 1995, Reddy and Srinath 1974, Horgan and Chan 1999, Chen *et al.* 2007). The stress analysis of rotating FGM cylinders are carried out by researchers (El-Naggar *et al.* 2002, Eraslan and Akis 2006, Wang 2010). Also, rotating piezoelectric disks and cylinders are concerned in many investigations. Babaei and Chen (2008a) presented the exact solution for electromechanical behavior of a rotating FGP hollow cylinder. Ghorbanpour Arani *et al.* (2011) studied the electro-thermo-mechanical behaviors of rotating FGP cylinder. Dai *et al.* (2012) presented the exact solution for stress distributions in a rotating FGP hollow cylinder for the case that properties of the material obey different power laws in the thickness direction.

Akbarzadeh *et al.* (2011) found that reducing the hoop stress by imposing a magnetic field is a capable way to increase the reliability of an FGPM cylinder. This is due to that the orthotropic piezoelectric cylinders have been observed to fail at a critical hoop stress (Galic and Horgan 2003). Recently, Dai *et al.* (2006, 2007, 2011a) studied the magnetothermoelastic interactions in hollow and solid cylindrical and spherical structures of FGM. Thermo-magneto-dynamic stresses in a non-homogeneous hollow cylinder was investigated (Kong *et al.* 2009; Wang and Dong 2006). Analytical solution for the electromagnetoelastic behavior of piezoelectric and FGPM hollow cylinder under magnetic, thermal, electrical, and mechanical loading are presented (Dai 2007, 2010). Babaei and Chen (2008b) presented the exact solutions for radially polarized and magnetized magneto-electroelastic rotating cylinders.

Furthermore, it is vital to analysis smart composite structures on elastic foundations for an accurate prediction of the structural behavior of smart materials. Ying *et al.* (2008) obtained the exact two-dimensional elastic solutions for the bending and free vibration of functionally graded beams on a Winkler–Pasternak elastic foundation. Kiani *et al.* (2012) studied the static, dynamic and free vibration behavior of FG doubly curved panels resting on a Pasternak-type elastic foundation. Akbarzadeh and Chen (2012) studied the Magneto-electro-elastic behavior of rotating solid and hollow cylinders resting on a Winkler elastic foundation under hygrothermal loading.

Imperfect interfacial bonding or delamination is a common type of flaw in laminated composite structures due to manufacturing defects or environmental conditions. Recently, the interlaminar bonding imperfections have been considered (Chen and Lee 2004, Chen *et al.* 2004). Kapuria and Nair (2010) investigated the exact three-dimensional piezothermoelasticity solution for dynamic behavior of rectangular cross-ply hybrid plates with bonding imperfections. Wang (2011) studied the dynamic electromechanical behavior of a triple-layer piezoelectric composite cylinder with imperfect interfaces using the linear spring model.

However, to the best of the authors' knowledge the electro-magneto-thermo-elastic analysis of a rotating long functionally graded hollow cylinder imperfectly bonded with functionally graded piezoelectric layers has not yet been reported. In the present study an analytical solution of a rotating FGM hollow cylinder with surface bounded functionally graded piezoelectric layers of infinite length under pressure, electrical excitation and thermal condition is presented. The mechanical boundary conditions also include the Winkler-type elastic foundation. The hybrid cylinder is placed in a constant magnetic field. A general linear spring-layer model is employed to describe the weakness of the imperfect interface between the FGM layer and the FGPM layers. The material properties of the FGM cylinder and radially polarized FGPM layers are assumed to be graded in the radial direction according to the power law. But, Poisson's ratio is assumed to be constant for FGM hollow cylinder. The hybrid cylinder is rotating about its axis at a constant angular velocity. The equations are solved analytically and the stresses and displacements and electric potential distributions are investigated. Numerical examples are given to show the influences of the material inhomogeneity, thermo-electro-mechanical boundary conditions, and magnetic field on the static behavior of smart FGM cylinder.

## 2. Basic formulations of the problem

An infinitely long hybrid functionally graded hollow cylinder (Fig. 1) with nonhomogeneous mechanical properties in the radial direction is considered. A cylindrical coordinate system  $(r, \theta, z)$  is used. The cylinder rotates about its axis at the constant angular velocity  $\omega$ . The hybrid cylinder is placed in a constant magnetic field  $H_0$  and subjected to an axisymmetric thermo-electro-mechanical loading. The cylinder could be rested on an elastic foundation with Winkler-type foundation stiffness  $K_w$  at the inner and/or outer surfaces or exposed to internal and/or external pressure.

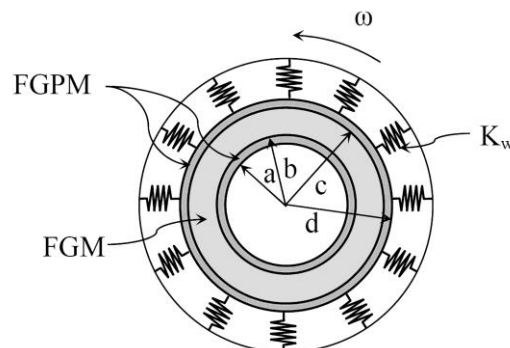


Fig. 1 Rotating FGM hollow cylinder with FGPM layers resting on an elastic foundation

### 2.1 Heat conduction problem

In this section, the symmetric, steady-state heat transfer equation is solved for the assumed boundary conditions in the cylindrical coordinate system for FGM cylinder bonded with two FGPM layers. The heat conduction equation in the steady-state condition for the one-dimension problem without internal heat source in the cylindrical coordinate is expressed as

$$\frac{1}{r} \frac{\partial}{\partial r} \left( rk(r) \frac{\partial T(r)}{\partial r} \right) = 0, \quad (a \leq r \leq d), \quad (1)$$

where  $k(r)$  is the thermal conduction coefficient of the hollow cylinder in the radial direction. Thermal conduction coefficient of FGM cylinder, inner FGPM layer and outer FGPM layer can be expressed as  $k(r) = k_{fgm} r^\eta$ ,  $k(r) = k_i r^\beta$  and  $k(r) = k_o r^\beta$ , respectively.  $\eta$  and  $\beta$  are inhomogeneity parameters of FGM and FGPM layers, respectively. Considering above expressions, Eq. (1) becomes

$$\frac{1}{r} \frac{\partial}{\partial r} \left[ r^{\theta+1} \frac{\partial T(r)}{\partial r} \right] = 0 \quad \theta = \beta, \eta. \quad (2)$$

By integrating twice, the solution of Eq. (2) for every layer can be expressed as

$$\begin{aligned} T_i(r) &= w_1^i r^{-\beta} + w_2^i, \\ T_{fgm}(r) &= w_3 r^{-\eta} + w_4, \\ T_o(r) &= w_1^o r^{-\beta} + w_2^o \end{aligned} \quad (3)$$

where  $T_i$ ,  $T_o$  and  $T_{fgm}$  are temperature distributions in the inner FGPM, outer FGPM and FGM layer, respectively.  $w_i$  ( $i=1, 2, 3, 4$ ) are unknown coefficients that can be found by applying boundary conditions. The linear spring model is considered due to the thermal field discontinuity (Kapuria and Nair 2010). The boundary conditions and continuity conditions can be expressed as

$$\begin{aligned} T_i(r)|_{r=a} &= T_0, \\ \left[ \frac{\partial T_o(r)}{\partial r} + hT_o(r) \right]_{r=d} &= 0, \\ q_i(r)|_{r=b} &= q_{fgm}(r)|_{r=b}, \\ q_o(r)|_{r=c} &= q_{fgm}(r)|_{r=c}, \\ T_i(r)|_{r=b} - T_{fgm}(r)|_{r=b} &= \chi_1 q_i(r)|_{r=b}, \\ T_{fgm}(r)|_{r=c} - T_o(r)|_{r=c} &= \chi_2 q_o(r)|_{r=c}. \end{aligned} \quad (4)$$

where  $h$  is the ratio of the convective heat-transfer coefficient of the cylinder and the surrounding medium,  $q_j$  ( $j=i, o, fgm$ ) are heat flux and  $\chi_1$  and  $\chi_2$  are the compliance constants of the inner and outer interfaces for thermal field. Clearly, for perfectly bonded interface, we have  $\chi_i = 0$  ( $i = 1, 2$ ).

Utilizing Eqs. (4)

$$\begin{aligned}
 w_0 &= \left[ hk_o \left( k_i \beta (\chi_2 \eta k_{fgm} - c) c^{(-\eta-1)} + \eta k_{fgm} (\chi_1 \beta k_i - b) b^{(-\eta-1)} + k_i \beta b^{(-\eta)} \right) c^{(-\beta-1)} \right. \\
 &\quad \left. - \eta k_i k_{fgm} \left( -\beta d^{(-\beta-1)} + h(d^{(-\beta)} - c^{(-\beta)}) \right) c^{(-\eta-1)} \right] b^{(-\beta-1)} + h \eta k_o k_{fgm} a^{(-\beta)} b^{(-\eta-1)} c^{(-\beta-1)} \\
 w_1^i &= \frac{h \eta k_o k_{fgm} b^{(-\eta-1)} c^{(-\beta-1)} T_0}{w_0} \\
 w_2^i &= \frac{(w_0 - h \eta k_o k_{fgm} b^{(-\eta-1)} c^{(-\beta-1)} a^{(-\beta)}) T_0}{w_0} \\
 w_3 &= \frac{h \beta k_i k_o b^{(-\beta-1)} c^{(-\beta-1)} T_0}{w_0} \\
 w_4 &= \frac{k_i T_0 \left( -\eta k_{fgm} \left( -\beta d^{(-\beta-1)} + h(d^{(-\beta)} - c^{(-\beta)}) \right) + h \beta k_o (\chi_2 \eta k_{fgm} - c) c^{(-\beta-1)} \right) b^{(-\beta-1)} c^{(-\eta-1)}}{w_0} \\
 w_1^o &= \frac{\eta k_{fgm} k_i h T_0 b^{(-\beta-1)} c^{(-\eta-1)}}{w_0} \\
 w_2^o &= - \frac{\eta k_i k_{fgm} T_0 \left( -\beta d^{(-\beta-1)} + h d^{(-\beta)} \right) b^{(-\beta-1)} c^{(-\eta-1)}}{w_0}
 \end{aligned} \tag{5}$$

## 2.2 FGM layer

In the symmetric state, the nonzero components of displacement and thermal distribution can be denoted as  $u = u(r)$  and  $T = T(r)$ . The equation of motion of the rotating long FGM hollow cylinder with perfect conductivity in plane strain state is expressed as

$$\frac{\partial \sigma_r}{\partial r} + \frac{\sigma_r - \sigma_\theta}{r} + f_z + \rho_f r \omega^2 = 0, \tag{6}$$

where  $\rho_f$  and  $\omega$  are the mass density and the angular velocity and  $f_z$  is defined as Lorentz's force, which for a constant magnetic field  $H_0$  may be written as (Akbarzadeh *et al.* 2011, Dai *et al.* 2010, 2011)

$$f_z = H_0^2 \frac{\partial}{\partial r} \left( \mu_f \left( \frac{\partial u}{\partial r} + \frac{u}{r} \right) \right), \tag{7}$$

where  $\mu_f$  is the magnetic permeability. By considering  $\varepsilon_r = \frac{du}{dr}$  and  $\varepsilon_\theta = \frac{u}{r}$ , the stress-displacement relations for FGM cylinder are

$$\begin{aligned}\sigma_r &= \frac{E(r)}{(1+\nu)(1-2\nu)} \left( (1-\nu) \frac{du}{dr} + \nu \frac{u}{r} \right) - \frac{E(r)\alpha(r)T(r)}{(1-2\nu)}, \\ \sigma_\theta &= \frac{E(r)}{(1+\nu)(1-2\nu)} \left( \nu \frac{du}{dr} + (1-\nu) \frac{u}{r} \right) - \frac{E(r)\alpha(r)T(r)}{(1-2\nu)}.\end{aligned}\quad (8)$$

In the FGM layer, the Poisson's ratio  $\nu$  is constant and the Young modulus, mass density, thermal expansion coefficient and magnetic permeability vary along the radial direction according to a power law as follows (Jabbari 2002)

$$E(r) = E_0 r^\eta, \quad \rho_f(r) = \rho_f^0 r^\eta, \quad \alpha(r) = \alpha_0 r^\eta, \quad \mu_f(r) = \mu_f^0 r^\eta, \quad (9)$$

where  $E_0$ ,  $\rho_f^0$ ,  $\alpha_0$  and  $\mu_f^0$  are material constants and  $\eta$  is the inhomogeneous constant. Substituting Eqs. (8) and (7) into Eq. (6) gives

$$\frac{d^2u}{dr^2} + (\eta+1) \frac{1}{r} \frac{du}{dr} + L_1 \frac{1}{r^2} u = -L_2 r + L_3 \left( 2\eta r^{\eta-1} T(r) + r^\eta \frac{dT(r)}{dr} \right), \quad (10)$$

where

$$\begin{aligned}L_1 &= \frac{E_0(\eta\nu - 1 + \nu) + (1+\nu)(1-2\nu)\mu_f^0 H_0^2(\eta-1)}{E_0(1-\nu) + (1+\nu)(1-2\nu)\mu_f^0 H_0^2}, \\ L_2 &= \frac{(1+\nu)(1-2\nu)\rho_f^0 \omega^2}{E_0(1-\nu) + (1+\nu)(1-2\nu)\mu_f^0 H_0^2}, \\ L_3 &= \frac{(1+\nu)E_0\alpha_0}{E_0(1-\nu) + (1+\nu)(1-2\nu)\mu_f^0 H_0^2}.\end{aligned}\quad (11)$$

Substituting from Eq. (3) into Eq. (10) yields

$$\frac{d^2u}{dr^2} + (\eta+1) \frac{1}{r} \frac{du}{dr} + L_1 \frac{1}{r^2} u = -L_2 r + L_3(\eta w_3 r^{-1} + 2\eta w_4 r^{\eta-1}) \quad (12)$$

Considering the basic displacement, complete solution of Eq. (12) may be expressed as following

$$u = u_g + u_p. \quad (13)$$

It is obvious that the homogeneous solution to Eq. (10) can be obtained by assuming

$$u_g = Qr^{\eta_i}, \quad (14)$$

where  $Q$  is an arbitrary constant. Substituting Eq. (14) into Eq. (12), one obtains

$$\eta_i^2 + \eta\eta_i + L_1 = 0. \quad (15)$$

Considering  $|\eta| \leq 2$ , only real distinct roots will be obtained. However, these values of  $\eta$  do not necessarily pertain to a certain material. Thus, various  $\eta$  values are used to demonstrate the effect of inhomogeneity on the results. Consequently, the characteristic Eq. (15) has two real roots  $\eta_1$  and  $\eta_2$  as follows

Now, the homogeneous solution to Eq. (12) can be expressed as

$$\eta_1 = -\frac{\eta}{2} + \sqrt{\frac{\eta^2}{4} - L_1}, \quad \eta_2 = -\frac{\eta}{2} - \sqrt{\frac{\eta^2}{4} - L_1}. \tag{16}$$

$$u_g = D_1 r^{\eta_1} + D_2 r^{\eta_2}, \tag{17}$$

where  $D_1$  and  $D_2$  are unknown constants determined by the given boundary conditions. The particular solution  $u_p(r)$  is

$$u_p = D_3 r + D_4 r^{\eta+1} + D_5 r^3, \tag{18}$$

where

$$\begin{aligned} D_3 &= \frac{\eta L_3 w_3}{\eta + 1 + L_1}, \\ D_4 &= \frac{2\eta L_3 w_4}{2\eta^2 + 3\eta + 1 + L_1}, \\ D_5 &= -\frac{L_2}{9 + 3\eta + L_1}. \end{aligned} \tag{19}$$

Utilizing Eqs. (17) and (18) we have

$$u(r) = D_1 r^{\eta_1} + D_2 r^{\eta_2} + D_3 r + D_4 r^{\eta+1} + D_5 r^3 \quad b \leq r \leq c. \tag{20}$$

Since  $u(r)$  is known, Eqs. (8) can be written as

$$\begin{aligned} \sigma_r &= \frac{E_0}{(1+\nu)(1-2\nu)} [((1-\nu)\eta_1 + \nu)D_1 r^{\eta_1+\eta-1} + ((1-\nu)\eta_2 + \nu)D_2 r^{\eta_2+\eta-1} \\ &\quad + (D_3 - (1+\nu)\alpha_0 w_3)r^\eta + ((\eta - \nu\eta + 1)D_4 - (1+\nu)\alpha_0 w_4)r^{2\eta} + D_5(3 - 2\nu)r^{2+\eta}], \\ \sigma_\theta &= \frac{E_0}{(1+\nu)(1-2\nu)} [(v\eta_1 + (1-\nu))D_1 r^{\eta_1+\eta-1} + (v\eta_2 + (1-\nu))D_2 r^{\eta_2+\eta-1} \\ &\quad + (D_3 - (1+\nu)\alpha_0 w_3)r^\eta + ((v\eta + 1)D_4 - (1+\nu)\alpha_0 w_4)r^{2\eta} + D_5(2\nu + 1)r^{2+\eta}]. \end{aligned} \tag{21}$$

### 2.3 FGPM layers

The inner and outer layers are radially polarized functionally graded piezoelectric material. For the cylindrically symmetric state, the nonzero components of displacement, temperature

distribution and electric potential can be denoted as  $u = u(r)$ ,  $T = T(r)$  and  $\varphi = \varphi(r)$ , respectively. The constitutive equations for FGPM layers in the reference coordinate system are (Saadatfar and Razavi 2009)

$$\begin{aligned}\sigma_r &= c_{12} \frac{u}{r} + c_{11} \frac{\partial u}{\partial r} + e_{11} \frac{\partial \varphi}{\partial r} - \lambda_1 T(r), \\ \sigma_\theta &= c_{22} \frac{u}{r} + c_{12} \frac{\partial u}{\partial r} + e_{12} \frac{\partial \varphi}{\partial r} - \lambda_2 T(r), \\ D_r &= e_{12} \frac{u}{r} + e_{11} \frac{\partial u}{\partial r} - g_{11} \frac{\partial \varphi}{\partial r} + p_{11} T(r),\end{aligned}\quad (22)$$

where  $\sigma_i(r)$  ( $i = r, \theta$ ) and  $D_r$  are components of stress and electric displacement, respectively.  $c_{ij}$ ,  $e_{ij}$ ,  $g_{11}$  and  $p_{11}$  are the elastic, piezoelectric, dielectric, pyroelectric, constants, respectively, and

$$\begin{aligned}\lambda_1 &= (c_{11}\alpha_r + c_{12}\alpha_\theta), \\ \lambda_2 &= (c_{12}\alpha_r + c_{22}\alpha_\theta),\end{aligned}\quad (23)$$

are thermal modulus where  $\alpha_i$  are thermal expansion coefficients. The equation of motion and the Maxwell equation in the absence of electric charge in the rotating piezoelectric layers are expressed as

$$\frac{\partial \sigma_r}{\partial r} + \frac{\sigma_r - \sigma_\theta}{r} + f_z + \rho_p r \omega^2 = 0, \quad (24a)$$

$$\frac{1}{r} \frac{\partial}{\partial r} [r D_r] = 0, \quad (24b)$$

where  $\rho_p$  is the mass density of FGPM layer and  $f_z$  is Lorentz's force, which may be written as

$$f_z = H_0^2 \frac{\partial}{\partial r} \left( \mu_p \left( \frac{\partial u}{\partial r} + \frac{u}{r} \right) \right) \quad (25)$$

All material constants are assumed to obey power-law equation through the radius of the FGPM layer, i.e.

$$\begin{aligned}c_{ij}(r) &= c_{ij}^0 r^\beta \quad (i = 1, 2; j = 1, 2), & e_{1i}(r) &= e_{1i}^0 r^\beta \quad (i = 1, 2), & g_{11}(r) &= g_{11}^0 r^\beta, \\ p_{11}(r) &= p_{11}^0 r^\beta, & \alpha_i(r) &= \alpha_i^0 r^\beta \quad (i = r, \theta), & \rho_{11}(r) &= \rho_p^0 r^\beta, & \mu_p(r) &= \mu_p^0 r^\beta\end{aligned}\quad (26)$$

where  $c_{ij}^0, e_{1i}^0, g_{11}^0, p_{11}^0, \alpha_i^0, \rho_p^0, \mu_p^0$  are material constants and  $\beta$  is the inhomogeneous constant. Now, Eqs. (23) become

$$\begin{aligned}\lambda_1 &= (c_{11}\alpha_r + c_{12}\alpha_\theta) = \lambda_1^0 r^{2\beta}, \\ \lambda_2 &= (c_{12}\alpha_r + c_{22}\alpha_\theta) = \lambda_2^0 r^{2\beta}.\end{aligned}\quad (27)$$

Solving Eqs. (24(b)), yields

$$D_r(r) = \frac{1}{r} A_1, \tag{28}$$

where  $A_1$  is an unknown constant. Substituting Eqs. (28) into the third equation of Eqs. (22), gives

$$\frac{\partial \phi(r)}{\partial r} = \frac{e_{11}^0}{g_{11}^0} \frac{\partial u}{\partial r} + \frac{e_{12}^0}{g_{11}^0} \frac{u}{r} + \frac{p_{11}^0}{g_{11}^0} T(r) - \frac{A_1}{g_{11}^0} \frac{1}{r^{\beta+1}}. \tag{29}$$

Substituting Eq. (29) into the first and second equations of Eqs. (22) yields

$$\begin{aligned} \sigma_r &= C_1 r^\beta \frac{\partial u}{\partial r} + C_2 r^\beta \frac{u}{r} + C_3 r^\beta T(r) - C_4 \frac{A_1}{r} - \lambda_1^0 r^{2\beta} T(r), \\ \sigma_\theta &= C_2 r^\beta \frac{\partial u}{\partial r} + C_5 r^\beta \frac{u}{r} + C_6 r^\beta T(r) - C_7 \frac{A_1}{r} - \lambda_2^0 r^{2\beta} T(r), \end{aligned} \tag{30}$$

where

$$\begin{aligned} C_1 &= c_{11}^0 + \frac{(e_{11}^0)^2}{g_{11}^0}, & C_2 &= c_{12}^0 + \frac{e_{11}^0 e_{12}^0}{g_{11}^0}, & C_3 &= \frac{e_{11}^0 p_{11}^0}{g_{11}^0}, & C_4 &= \frac{e_{11}^0}{g_{11}^0}, \\ C_5 &= c_{22}^0 + \frac{(e_{12}^0)^2}{g_{11}^0}, & C_6 &= \frac{e_{12}^0 p_{11}^0}{g_{11}^0}, & C_7 &= \frac{e_{12}^0}{g_{11}^0}. \end{aligned} \tag{31}$$

Substituting Eqs. (30) and (25) into Eq. (24(a)), the motion equation is expressed as

$$\begin{aligned} \frac{\partial^2 u}{\partial r^2} + (1 + \beta) \frac{1}{r} \frac{\partial u}{\partial r} + W_1 \frac{u}{r^2} &= W_2 r^\beta \frac{T(r)}{r} + W_3 \frac{T(r)}{r} + W_4 r^\beta \frac{\partial T(r)}{\partial r} \\ &+ W_5 \frac{\partial T(r)}{\partial r} + W_6 A_1 r^{-\beta-2} + W_7 r, \end{aligned} \tag{32}$$

where

$$\begin{aligned} W_1 &= \frac{C_2 \beta - C_5 + \mu_p^0 H_0^2 (\beta - 1)}{C_1 + \mu_p^0 H_0^2}, & W_2 &= \frac{2\lambda_1^0 \beta + \lambda_1^0 - \lambda_2^0}{C_1 + \mu_p^0 H_0^2}, \\ W_3 &= \frac{C_6 - C_3 \beta - C_3}{C_1 + \mu_p^0 H_0^2}, & W_4 &= \frac{\lambda_1^0}{C_1 + \mu_p^0 H_0^2}, & W_5 &= \frac{-C_3}{C_1 + \mu_p^0 H_0^2}, \\ W_6 &= \frac{-C_7}{C_1 + \mu_p^0 H_0^2}, & W_7 &= \frac{-\rho_p^0 \omega^2}{C_1 + \mu_p^0 H_0^2} \end{aligned} \tag{33}$$

Substituting the first equation of Eqs. (3) into Eq. (32), yields

$$\frac{\partial^2 u}{\partial r^2} + (1 + \beta) \frac{1}{r} \frac{\partial u}{\partial r} + W_1 \frac{u}{r^2} = W_9 r^{-1} + W_{10} r^{\beta-1} + W_{11} r^{-\beta-1} + W_6 A_1 r^{-\beta-2} + W_7 r, \tag{34}$$

where (for inner FGPM layer)

$$W_9 = W_2 w_1^i + W_3 w_2^i - W_4 w_1^i \beta, \quad W_{10} = W_2 w_2^i, \quad W_{11} = W_3 w_1^i - W_5 w_1^i \beta. \quad (35)$$

The homogenous solution of Eq. (34) can be expressed as

$$u_g(r) = B_1 r^{\beta_1} + B_2 r^{\beta_2}, \quad (36)$$

where  $B_1$  and  $B_2$  are unknown constants determined by the given boundary conditions, and

$$\beta_1 = \frac{1}{2}(-\beta + \sqrt{\beta^2 - 4W_1}), \quad \beta_2 = \frac{1}{2}(-\beta - \sqrt{\beta^2 - 4W_1}). \quad (37)$$

The particular solution  $u_p(r)$  is in the following form

$$u_p(r) = B_3 r + B_4 r^{\beta+1} + B_5 r^{-\beta+1} + B_6 r^3 + \frac{W_6 A_1}{W_1} r^{-\beta}, \quad (38)$$

where

$$\begin{aligned} B_3 &= \frac{W_9}{\beta+1+W_1}, & B_4 &= \frac{W_{10}}{2\beta^2+3\beta+1+W_1}, \\ B_5 &= \frac{W_{11}}{-\beta+1+W_1}, & B_6 &= \frac{W_7}{9+3\beta+W_1}. \end{aligned} \quad (39)$$

Utilizing Eqs. (36) and (38) we have

$$u(r) = B_1 r^{m_1} + B_2 r^{m_2} + B_3 r + B_4 r^{\beta+1} + B_5 r^{-\beta+1} + B_6 r^3 + \frac{W_6 A_1}{W_1} r^{-\beta} \quad a \leq r \leq b. \quad (40)$$

Since  $u(r)$  is known, by integrating from the Eq. (29)

$$\begin{aligned} \varphi(r) &= C_4 \left[ B_1 r^{\beta_1} + B_2 r^{\beta_2} + B_3 r + B_4 r^{\beta+1} + B_5 r^{-\beta+1} + B_6 r^3 + \frac{W_6 A_1}{W_1} r^{-\beta} \right] \\ &+ C_7 \left[ \frac{B_1}{\beta_1} r^{\beta_1} + \frac{B_2}{\beta_2} r^{\beta_2} + B_3 r + \frac{B_4}{\beta+1} r^{\beta+1} + \frac{B_5}{-\beta+1} r^{-\beta+1} + \frac{B_6}{3} r^3 + \frac{W_6 A_1}{W_1(-\beta)} r^{-\beta} \right] \\ &+ \frac{p_{11}^0}{g_{11}^0} \left( \frac{w_1^i}{-\beta+1} r^{-\beta+1} + w_2^i r \right) - \frac{A_1}{g_{11}^0 \beta} r^{-\beta} + A_2, \end{aligned} \quad (41)$$

where  $A_2$  is an unknown constant. Substituting Eq. (40) into Eqs. (30), the stresses of the inner FGPM layer are obtained as

$$\begin{aligned} \sigma_r = & C_1 r^\beta \left[ B_1 \beta_1 r^{\beta_1-1} + B_2 \beta_2 r^{\beta_2-1} + B_3 + B_4 (\beta + 1) r^\beta + B_5 (1 - \beta) r^{-\beta} + 3B_6 r^2 - \frac{\beta W_6 A_1}{W_1} r^{-\beta-1} \right] \\ & + C_2 r^\beta \left[ B_1 r^{\beta_1-1} + B_2 r^{\beta_2-1} + B_3 + B_4 r^\beta + B_5 r^{-\beta} + B_6 r^2 + \frac{W_6 A_1}{W_1} r^{-\beta-1} \right] - C_4 \frac{A_1}{r} \\ & + (C_3 r^\beta - \lambda_1^0 r^{2\beta})(w_1^i r^{-\beta} + w_2^i), \end{aligned} \tag{42a}$$

$$\begin{aligned} \sigma_\theta = & C_2 r^\beta \left[ B_1 \beta_1 r^{\beta_1-1} + B_2 \beta_2 r^{\beta_2-1} + B_3 + B_4 (\beta + 1) r^\beta + B_5 (1 - \beta) r^{-\beta} + 3B_6 r^2 - \frac{\beta W_6 A_1}{W_1} r^{-\beta-1} \right] \\ & + C_5 r^\beta \left[ B_1 r^{\beta_1-1} + B_2 r^{\beta_2-1} + B_3 + B_4 r^\beta + B_5 r^{-\beta} + B_6 r^2 + \frac{W_6 A_1}{W_1} r^{-\beta-1} \right] - C_7 \frac{A_1}{r} \\ & + (C_6 r^\beta - \lambda_2^0 r^{2\beta})(w_1^i r^{-\beta} + w_2^i), \end{aligned} \tag{42b}$$

The displacement, stresses and electric potential of the outer FGPM layer can be obtained by the same way just by replacing  $w_1^i$  and  $w_2^i$  by  $w_1^o$  and  $w_2^o$  in the Eq. (35) up to Eq. (42), respectively. The hybrid hollow cylinder may be simulated with or without a Winkler elastic foundation on the inner and/or outer surfaces. So, the elastic boundary conditions can be considered as follows (Akbarzadeh and Chen 2013)

- Internal and external pressure

$$\sigma_r^{ip} \Big|_{r=a} = -p_i, \quad \sigma_r^{op} \Big|_{r=d} = -p_o, \tag{43a}$$

- Internal pressure and elastic foundation on the outer surface

$$\sigma_r^{ip} \Big|_{r=a} = -p_i, \quad \sigma_r^{op} \Big|_{r=d} = -K_w u_r^{op} \Big|_{r=d} \tag{43b}$$

- Elastic foundation on the inner surface and external pressure

$$\sigma_r^{ip} \Big|_{r=a} = K_w u_r^{ip} \Big|_{r=a}, \quad \sigma_r^{op} \Big|_{r=d} = -p_o \tag{43c}$$

- Elastic foundation on both the inner and outer surfaces

$$\sigma_r^{ip} \Big|_{r=a} = K_w u_r^{ip} \Big|_{r=a}, \quad \sigma_r^{op} \Big|_{r=d} = -K_w u_r^{op} \Big|_{r=d} \tag{43d}$$

Furthermore, the electrical boundary conditions can be expressed as

$$\begin{aligned} \varphi^{ip} \Big|_{r=a} &= \varphi_a, & \varphi^{ip} \Big|_{r=b} &= \varphi_b, \\ \varphi^{op} \Big|_{r=c} &= \varphi_c, & \varphi^{op} \Big|_{r=d} &= \varphi_d, \end{aligned} \tag{44}$$

where superscripts ip, op and fgm denote parameters in the inner FGPM, outer FGPM and FGM layers, respectively.

For piezoelectric composites under mechanical and electrical loading, the interface might be mechanically and/or electrically imperfect. It is found that the mechanical imperfection has more

significant effect on the behavior of the smart composite (Li and Lee 2009, Chen and Lee 2005). In this work, only the mechanical imperfection is considered. The linear spring-layer model is applied to describe the imperfect bonding (Wang 2011, Chen and Lee 2005). Thus

$$\begin{aligned}
 \sigma_r^{ip} \Big|_{r=b} &= \sigma_r^{fgm} \Big|_{r=b} \\
 \sigma_r^{op} \Big|_{r=c} &= \sigma_r^{fgm} \Big|_{r=c} \\
 u_r^{fgm} \Big|_{r=b} - u_r^{ip} \Big|_{r=b} &= \zeta_1 \sigma_r^{ip} \Big|_{r=b} \\
 u_r^{op} \Big|_{r=c} - u_r^{fgm} \Big|_{r=c} &= \zeta_2 \sigma_r^{fgm} \Big|_{r=c}
 \end{aligned} \tag{45}$$

where  $\zeta_1$  and  $\zeta_2$  are the compliance constants of the inner and outer interfaces for mechanical field. Clearly, for perfectly bonded interface, we have  $\zeta_i = 0$  ( $i = 1, 2$ ). Unknown coefficients ( $A_1, A_2, B_1$  and  $B_2$  coefficients for inner FGPM layer and also four coefficients for outer FGPM layer and  $D_1$  and  $D_2$  for FGM layer) can be found by applying mechanical and electrical boundary conditions and interfacial conditions. For each case of boundary conditions, the system of ten linear algebraic equations for the unknown constants can be written in the following form

$$X \begin{bmatrix} B_1 & B_2 & A_1 & A_2 & D_1 & D_2 & B_1' & B_2' & A_1' & A_2' \end{bmatrix}^T = F, \tag{46}$$

where  $A_1', A_2', B_1'$  and  $B_2'$  are unknown coefficients for the outer FGPM layer and X and F are known matrix that their components are given in the appendix section. By solving the Eq. (46), the solution procedure is completed and stresses, displacement and electric potential are obtained analytically.

### 3. Numerical results and discussions

Considering numerical calculations, material constants for the hybrid hollow cylinder are listed in Table 1 (Alibeigloo 2008, Xiang and Shi 2009, Akbarzadeh and Chen 2012). A hybrid hollow cylinder with internal radius  $a = 0.6$  m and external radius  $d = 1$  m is considered. The thickness of each FGPM layer is 0.02 m. To study the influences of effective parameters (unless imperfection) on the behavior of hybrid cylinder, the layers are assumed perfectly bonded to each other ( $\chi_1 = \chi_2 = \zeta_1 = \zeta_2 = 0$ ). The cylinder rotates at constant angular velocity of  $\omega = 6\pi$ . The hybrid cylinder is placed in a constant magnetic field  $H_0 = 0.2 \times 10^9$ . The temperature on the inner surface and foundation stiffness on the outer surface are considered as  $T_0 = 50$  K and  $K_w = 600 \times 10^9$ . Considering pressure on the inner surface and elastic foundation on the outer surface (Eq. (43(b))), the other corresponding boundary conditions are expressed as

$$P_i = 1 \times 10^9 \text{ Pa}, \quad \phi_a = 0, \quad \phi_b = 0, \quad \phi_c = 0, \quad \phi_d = 0.$$

The following non-dimensional quantities are introduced

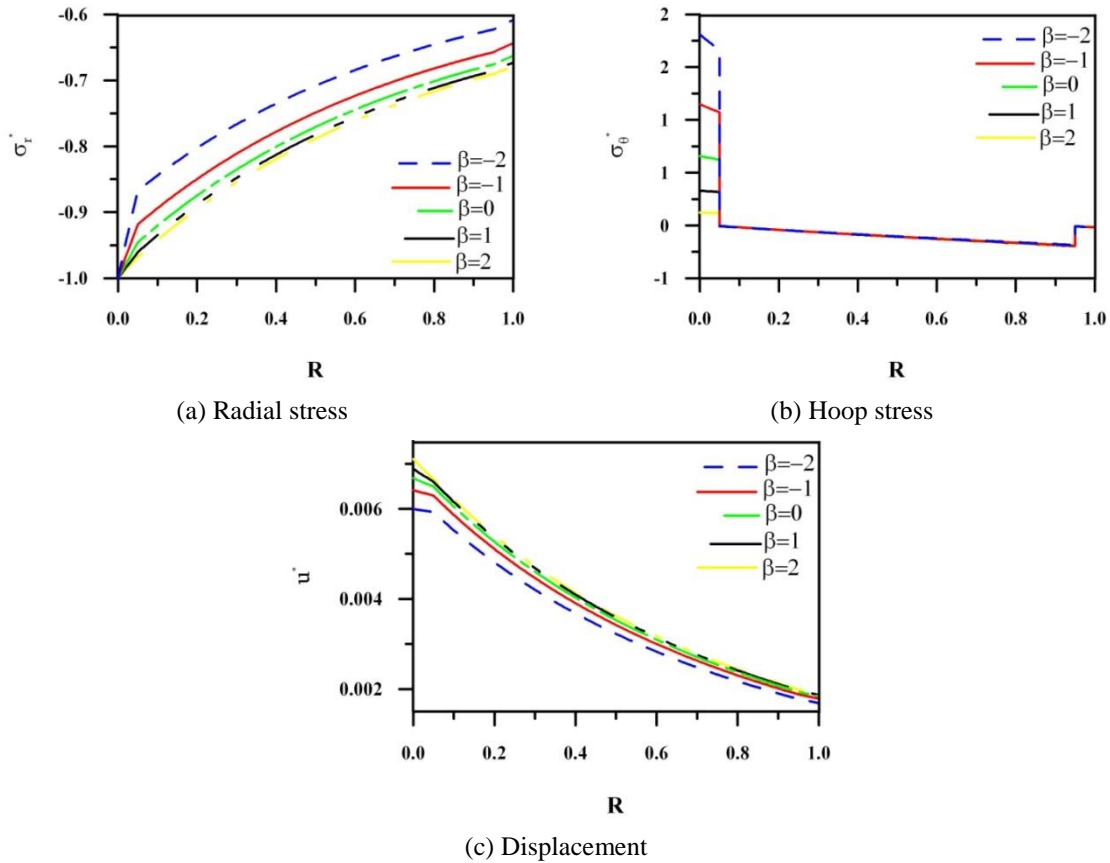


Fig. 2 Variations of radial stress, hoop stress and displacement distributions for different  $\beta$ ,  $\eta=2$

$$R = \frac{r-a}{d-a}, \quad u^* = \frac{u(r)}{a}, \quad \sigma_j^* = \frac{\sigma_j}{P_i}, \quad (j = r, \theta).$$

The effect of gradient index ( $\beta$ ) of FGPM layers on the behavior of smart cylinder is presented in Fig. 2. It can be observed that the interface continuity conditions and boundary conditions are satisfied. As it is expected, by decreasing the displacement in the outer surface of the cylinder, the radial stress in the outer surface reduces due to elastic foundation. The radial stress and displacement are decreasing with the decreasing of  $\beta$ . The decrease in the inner surface of FGM is more intensive than the outer surface.

This is worth noting that decreasing the  $\beta$  value in the inner FGPM layer reduces the radial stress and displacement. However, this is less effective in the outer FGPM layer. The effect of gradient index on the radial stress is greater than that of the displacement. So, the stresses and displacement in FGM layer can be controlled more effectively by using functionally graded piezoelectric material with suitable gradient index rather than homogenous piezoelectric. Considering Fig. 2(b), the circumferential stress in the FGM layer and outer FGPM layer is almost constant with different  $\beta$  but in the inner FGPM layer it increased with the decreasing of  $\beta$ .

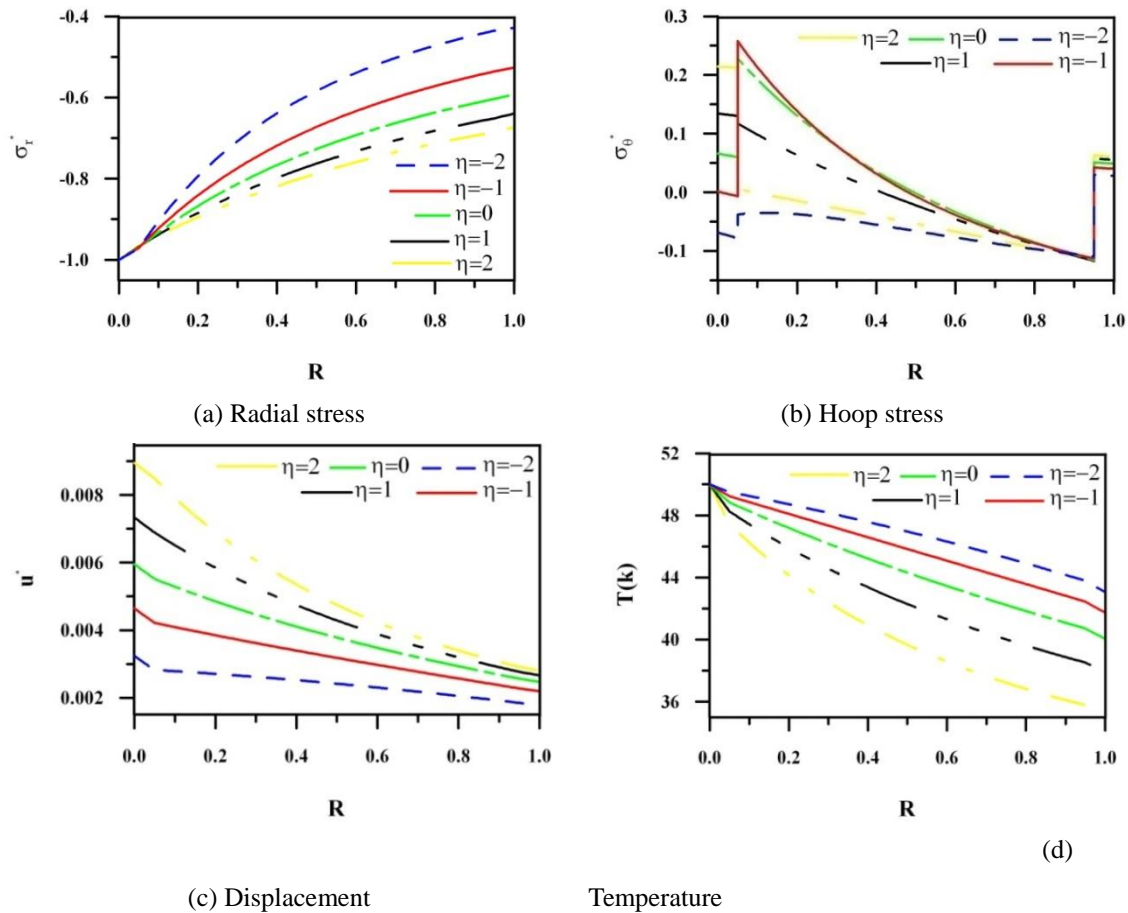


Fig. 3 Variations of radial stress, hoop stress, displacement and temperature distributions for different  $\eta$ ,  $\beta=2$

The effect of gradient index ( $\eta$ ) of FGM layer on the behavior of hybrid cylinder is presented in Fig. 3. The foundation stiffness is considered as  $K_w = 400 \times 10^9$ . All other conditions remain unchanged. Fig. 3(a) depicts the distribution of radial stress along the radius for different values of  $\eta$ . It is clear that the radial stresses at the internal and the external surfaces of the hollow rotating cylinder satisfy the given boundary conditions. Moreover, the magnitude of the radial stress is increased as  $\eta$  is increased. Similar to the previous case, by decreasing the displacement in the outer surface of the cylinder, the magnitude of the radial stress in the outer surface reduced due to the elastic foundation. It can be observed (Fig. 3(b)) that we can significantly decrease the hoop stress in the inner surface of FGM layer ( $\eta=2$ ) by use of a proper gradient index. Furthermore, we can obtain compressive hoop stress in the FGM layer and inner FGPM layer by considering a suitable gradient index ( $\eta=-2$ ).

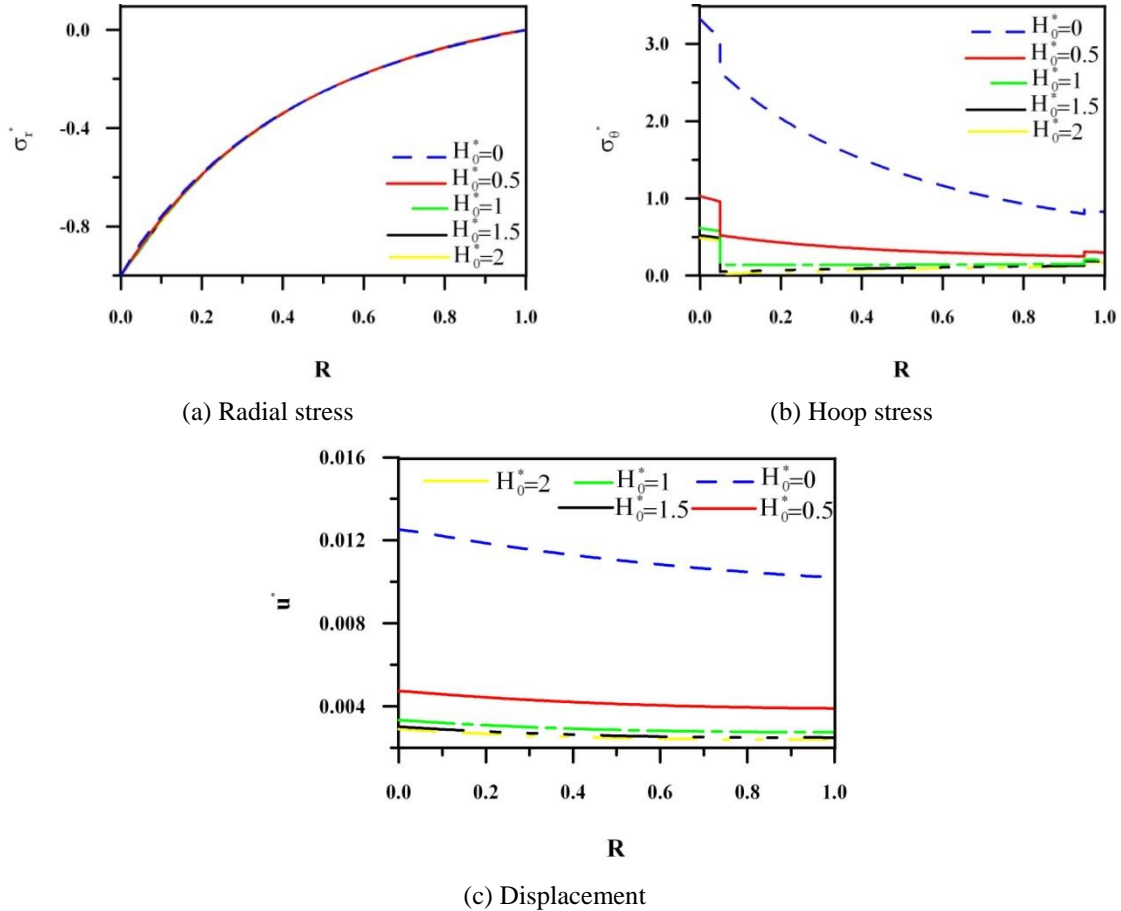


Fig. 4 Variations of radial stress, hoop stress and displacement distributions for different  $H_0^*$ ,  $\eta=\beta=-1.5$

Besides, it is observed that the hoop stress in the outer surface of the FGM layer is almost constant with different  $\eta$ . Figs. 3(c) and 3(d) show that the thermal boundary conditions and continuity conditions and also the displacement continuity conditions is satisfied. It is clear that the displacement increases and the outer temperature decreases with increasing  $\eta$ . Furthermore, increasing of  $\eta$  increases the displacement of the inner surface more than the outer surface. It seems that for reducing the magnitude of the radial stress and displacement at any point it is necessary to use a FGM shell with a hard inner surface.

Fig. 4 shows the effects of magnetic field on the distribution of stresses and displacement along the radial direction of the hybrid cylinder under the boundary conditions that are expressed according to the Eq. (43(a)) and without any external pressure ( $\eta=-1.5$  and  $\beta=-1.5$ ). All other conditions remain unchanged. It can be observed that the influence of  $H_0$  on the radial stress is negligible ( $H_0=H_0^* \times 10^9$  (A/m)). Figs. 4(b) and 4(c) show that imposing the magnetic field resulted in significant decrease of the hoop stress and displacement. It is clear that by increasing  $H_0$ , the displacement decreases and the hoop stress in FGM layer vanishes ( $H_0^*=2$ ). Consequently,

imposing a proper magnetic field reduces the hoop stress and displacement in a rotating hybrid FGM cylinder. This results in a smart structure that is more reliable. Moreover, increasing  $H_0$  decreases the hoop stress of the inner surface of the FGM layer more than the outer surface. It seems that the influence of imposing magnetic field becomes negligible when  $H_0 > 1.5 \times 10^9$  (A/m).

Fig. 5 show an interesting case in which  $\eta=1.5$  and  $\beta=-1.5$ . It is interesting to note that unlike the Fig. 4(a), the effect of magnetic field on the radial stress is considerable. It can be seen that the interface continuity conditions and boundary conditions are satisfied completely. As it is shown in Fig. 5(a), the radial stress in the FGM layer significantly reduces by imposing a suitable magnetic field. It seems that there exists a fixed point at which the value of radial stress does not change with varying the magnetic field. Increasing the magnetic field decreases the magnitude of the radial stress on the inner surface and increases it on the outer surface of the FGM layer. Figs. 5(b) and 5(c) show that, unlike Figs. 4(b) and 4(c), imposing the magnetic field increases the hoop stress and displacement. Concerning Figs. 4 and 5, it is possible to obtain various static behaviors of smart FGM cylinder by applying a suitable gradient index ( $\eta$ ) and imposing proper magnetic fields.

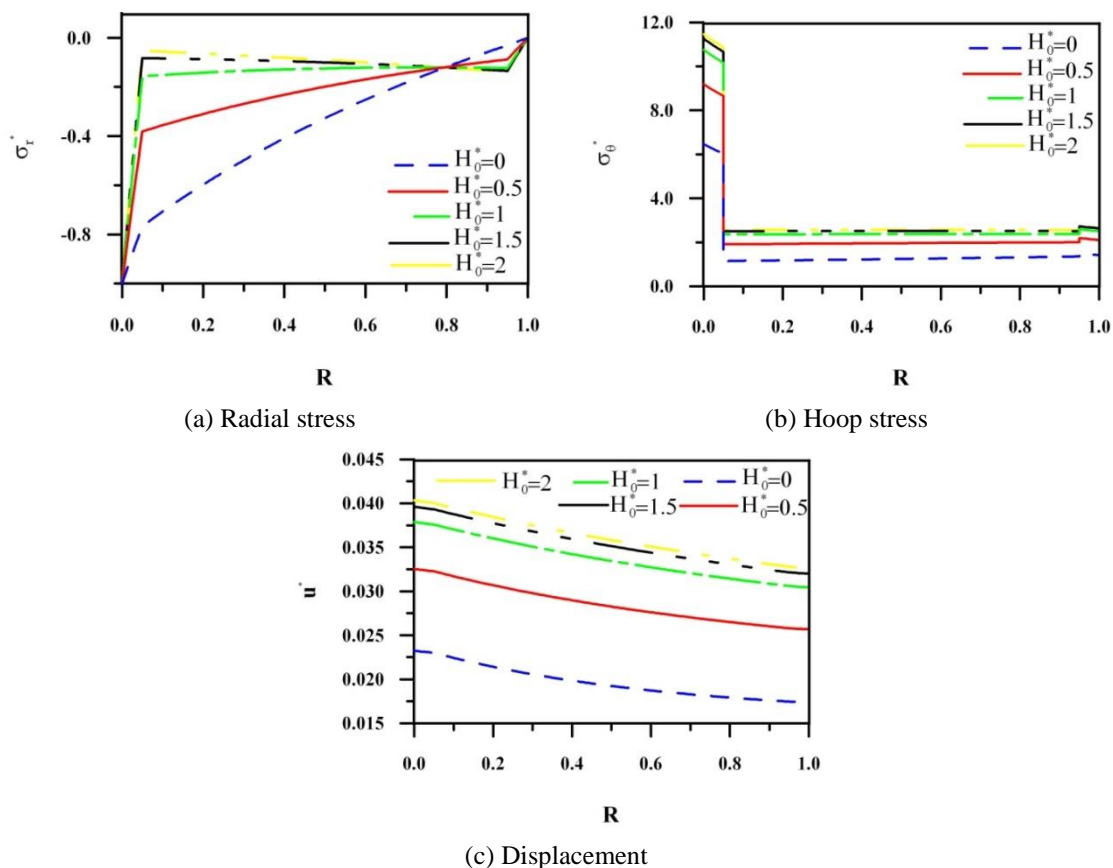


Fig. 5 Variations of radial stress, hoop stress and displacement distributions for different  $H_0^*$ ,  $\eta=1.5$ ,  $\beta=-1.5$

Table 1 Materials constants

FGM				
$E_0$ (GPa)	$\alpha_0$ (1/K)	$k_{fgm}$ (W/mK)	$\rho_f^0$ (kg / m <sup>3</sup> )	$\mu_f^0$ (H / m)
125	$10 \times 10^{-6}$	2.9	7860	$4\pi \times 10^{-7}$
FGPM				
$c_{11}^0$ (GPa)	$c_{12}^0$ (GPa)	$c_{22}^0$ (GPa)	$e_{11}^0$ (C / m <sup>2</sup> )	$e_{12}^0$ (C / m <sup>2</sup> )
139	78	139	15.1	-5.2
$k_i$ (W/mK)	$k_0$ (W/mK)	$P_{11}^0$ (C <sup>2</sup> / m <sup>2</sup> k)	$g_{11}^0$ (C <sup>2</sup> / N m <sup>2</sup> )	$\rho_p^0$ (kg / m <sup>3</sup> )
1.5	1.5	$-3.2 \times 10^{-5}$	$5.6 \times 10^{-9}$	7750
$\alpha_r^0$ (1 / K)	$\alpha_\theta^0$ (1 / K)	$h$ (W / m <sup>2</sup> K)	$\mu_p^0$ (H / m)	
$8.53 \times 10^{-6}$	$1.99 \times 10^{-6}$	0.82	$4\pi \times 10^{-7}$	

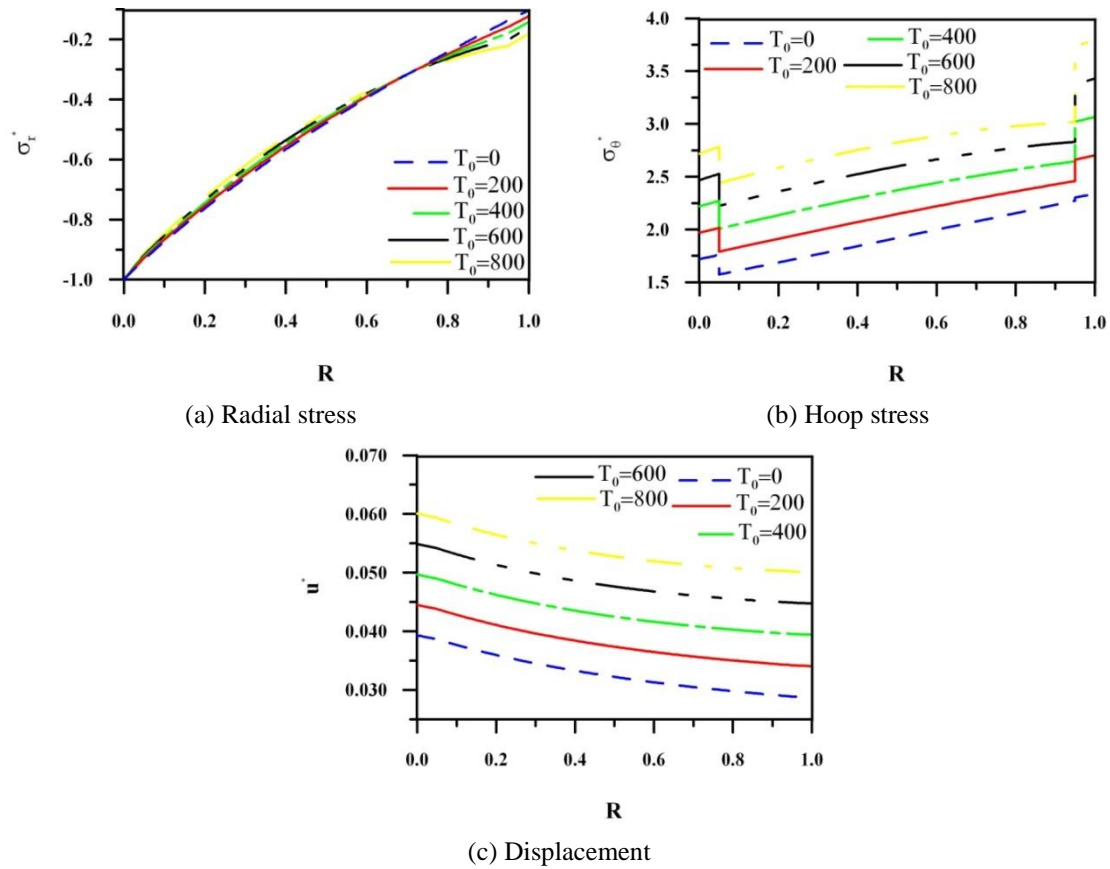


Fig. 6 Effect of inner temperature on radial stress, hoop stress and displacement distributions,  $\eta=2, \beta=2$

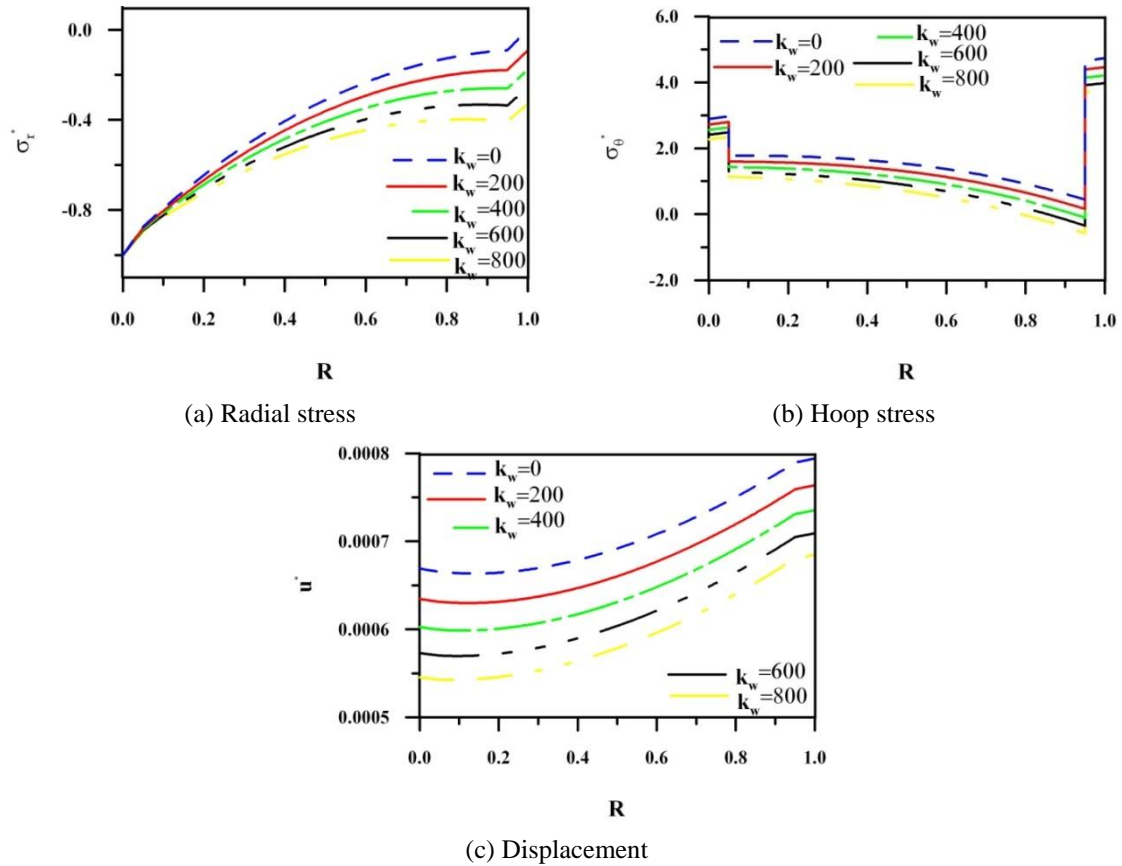


Fig. 7 Influence of elastic foundation on radial stress, hoop stress and displacement distributions,  $\eta=\beta=2$

The effect of internal temperature ( $T_0$ ) of hybrid cylinder on the stresses and displacement is presented in Fig. 6. In this case, the elastic foundation on the outer surface is considered based on Eq. (43(b)). In this case, the foundation stiffness is considered as  $K_w = 600 \times 10^7$ . All other conditions remain unchanged. Fig. 6a shows that there exists a fixed point at  $R=0.698$  at which the value of radial stress does not change with altering the inner temperature. Before this point, increasing the inner temperature leads to an increase in the radial stress while after this point the behavior of the radial stress is reversed. By reducing the displacement in the outer surface of the cylinder, the radial stress in the outer surface reduces because of the elastic foundation. Figs. 6(b) and 6(c) show that raising the temperature on the inner surface increases the hoop stress and displacement in the hybrid cylinder.

The effect of elastic foundation on the behavior of the FG smart cylinder under boundary conditions that are described based on the Eq. (43(b)) is shown in Fig. 7. In this case, the internal pressure is  $P_i=1 \times 10^7$  Pa and the magnetic field is not considered ( $H_0=0$ ). All other conditions remain unchanged ( $K_w=k_w \times 10^7$ ). Fig. 7(a) shows that an increase in the stiffness of the foundation results in an increase in the absolute value of the through thickness radial stresses. This is

reasonable that the presence of an elastic foundation helps to suppress the radial displacement and results in a compressive radial stress on the outer surface. It is valuable to note that,  $k_w = 0$  simulates the situation in which the cylinder is traction free on the outer surface. Figs. 7(b) and 7(c) show that the hoop stress and the displacement decrease with increasing of the foundation stiffness. This was predictable that the presence of an elastic foundation helps to resist the radial displacement due to the outward radial displacement of the outer surface.

The effect of applied voltage (in unit of volt) on the stresses and displacement of the cylinder under complex load is shown in Fig. 8. In this case,  $\omega=2\pi$ ,  $P_i=1\times 10^5$  Pa,  $H_0=0.2\times 10^5$  (A/m),  $k_w=0$  and  $T_0=0$  K. It can be observed that the displacement and the hoop stress decrease by applying voltage in the inner FGPM layer and increase by applying voltage in the outer FGPM layer. It is also clear that the displacement and hoop stress are decreasing with increasing of the applied voltage in the inner FGPM layer. Thus, it can be concluded that the inner FGPM layer is more suitable for using as an actuator than the outer FGPM layer. The induced strain of the FGPM actuator layer caused by applied voltage can vary the stress and displacement distributions of the cylinder. Considering Fig. 8, the values of mechanical quantities can be controlled by applying voltage in actuator layer.

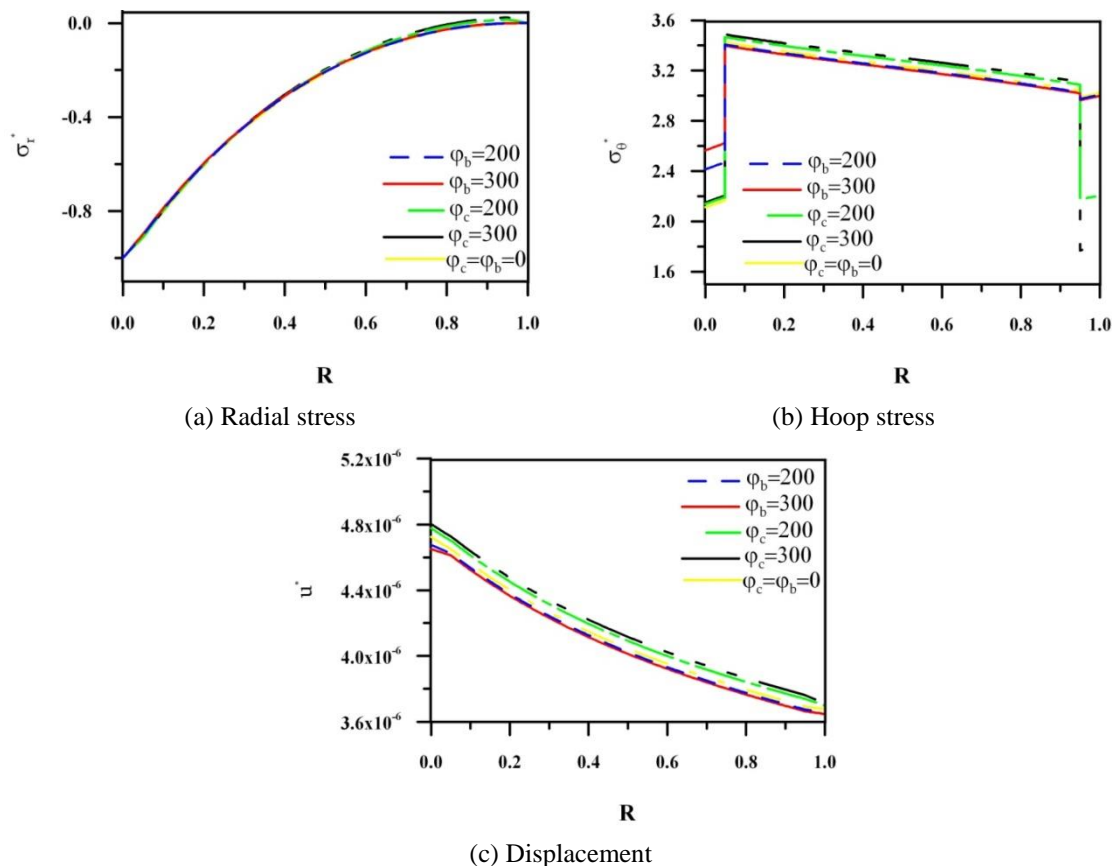


Fig. 8 Influence of applied voltage on radial stress, circumferential stress and displacement distributions,  $\eta=1$ ,  $\beta=2$

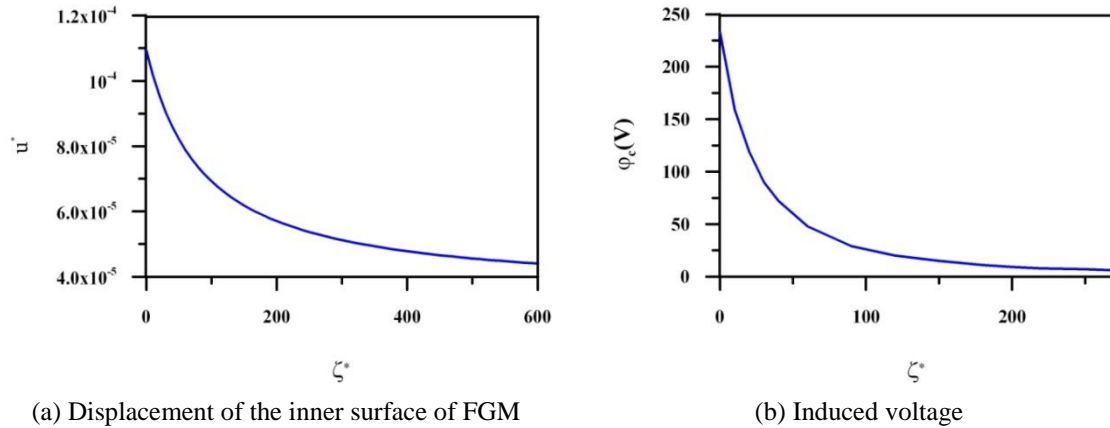


Fig. 9 Influence of imperfect bonding on actuation authority and sensory potential,  $\eta = \beta = 1.5$ ,  $\eta = 1$ ,  $\beta = 2$

The effects of imperfect bonding on the behavior of hybrid cylinder are depicted in Fig. 9. Actuation authority and sensory potential are important parameters that are affected by imperfection in piezoelectric composites (Kapuria and Nair 2010). So, only the effect of imperfect bonding on the actuation authority and sensory potential of FGPM layers is considered here. The compliance coefficients at an imperfect interface are taken as  $\zeta_1 = \zeta_2 = \zeta^*/(139 \times 10^9)$  and  $\chi_1 = \chi_2 = \zeta^*/290$ . The inner and outer FGPM layer are considered as actuator and sensor, respectively. As a first case, no any mechanical load is applied on the cylinder and other parameters are considered as  $\omega = 0$ ,  $P_i = 0$ ,  $H_0 = 0$ ,  $k_w = 0$  and  $T_0 = 20$  K. An electrical load of  $\phi_a = 200$  V is considered as actuation load.

Fig. 9(a) depicts the displacement of the inner surface of the FGPM layer through the compliance coefficient of the imperfect bonding. It is observed that the actuation capability of the actuator decreases by increasing the compliance coefficient of the imperfection. Concerning higher values of imperfection, the difference among the results is not appreciable. As a second case, no any electrical load is applied on the cylinder and other parameters are considered as  $\omega = 0$ ,  $P_i = 5 \times 10^5$  Pa,  $H_0 = 0$ ,  $k_w = 0$  and  $T_0 = 50$  K. The effect of imperfection on the induced voltage is presented in Fig. 9(b). As it is expected, the measured voltage ( $\phi_c$ ) in sensor decreases by increasing the compliance coefficient of imperfection. For large values of  $\zeta^*$ , the curve becomes nearly flat representing no further significant change in the measured voltage.

In order to validate analytical results, the present analysis results are tried to be compared with reported results in the literature. It is worth noting that there are no published results in the open literature concerning multifield analysis involving magneto-thermo-electroelastic behavior of a long FGM cylinder with FGPM layers. Thus, the present analysis is compared with electro-magneto-thermoelastic analysis in a FGM (Dai *et al.* 2011b) hollow cylinder and electroelastic analysis of rotating FGPM (Babaei and Chen 2008a) hollow cylinder. It should be mentioned that effects of piezoelectric layers on the response of FGM layer should be ignored if the thickness of piezoelectric layers become less than 2% of the cylinder thickness (Alibeigloo 2011). Considering analysis of one layer FGM and/or FGPM hollow cylinder, the thickness of other layers can be assumed less than 0.001 of the thickness of main layer. The mechanical boundary conditions are expressed as  $p_i = 30 \times 10^6$  Pa and  $p_o = 0$  Pa, and the temperature of internal

boundary is assumed to be  $T_0=10^\circ\text{C}$ . Material constants can be found in Dai *et al.* (2011b). Other parameters are taken as:  $b=0.1\text{ m}$ ,  $c=0.2\text{ m}$ ,  $H_z=2.23\times 10^9\text{ (A/m)}$ ,  $h=0.72\text{ W/mK}$  and  $\omega=0$ . Distributions of temperature and displacement are depicted in Fig. 10. It can be observed that the obtained results are fairly well correlated to Dai (2011b).

Concerning one layer rotating FGPM hollow cylinder, dimensionless quantities are taken as:  $R = \frac{r}{a}$ ,  $u^* = \frac{u(r)}{a}$ ,  $\sigma_j^* = \frac{\sigma_j}{c_{11}^0}$ , ( $j = r, \theta$ ),  $\Phi = \frac{e_{11}}{ac_{11}^0}\phi$ ,  $\Omega = \frac{\rho\omega^2 a^2}{c_{11}}$ . The electromechanical boundary conditions are considered as:  $\sigma_r^*|_{r=a} = 1$ ,  $\sigma_r^*|_{r=b} = 0$ ,  $\Phi_a=1$  and  $\Phi_b=0$ . Material constants can be found in Babaei and Chen (2008a). The distributions of radial and circumferential stresses for  $\Omega=1$  are depicted in Fig. 11. It is observed that results obtained are in good agreement with Babaei and Chen (2008a). It is worthwhile to mention that multiphysical closed-form solutions in previous section and graphical results in this section could be used as a benchmark solution for magneto-thermo-electroelastic analysis of hybrid composite cylinders.

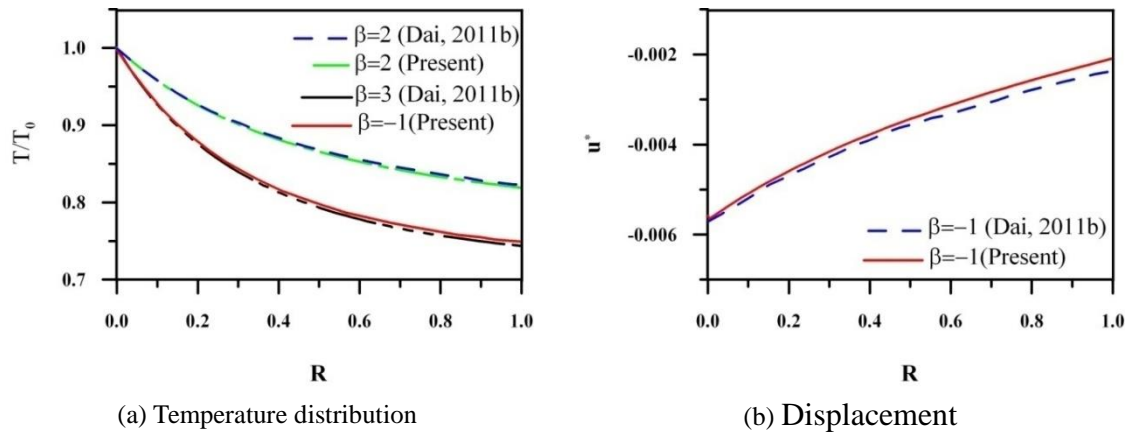


Fig. 10 Temperature distribution and displacement in FGM Hollow cylinder subjected to magneto-thermoelastic loading

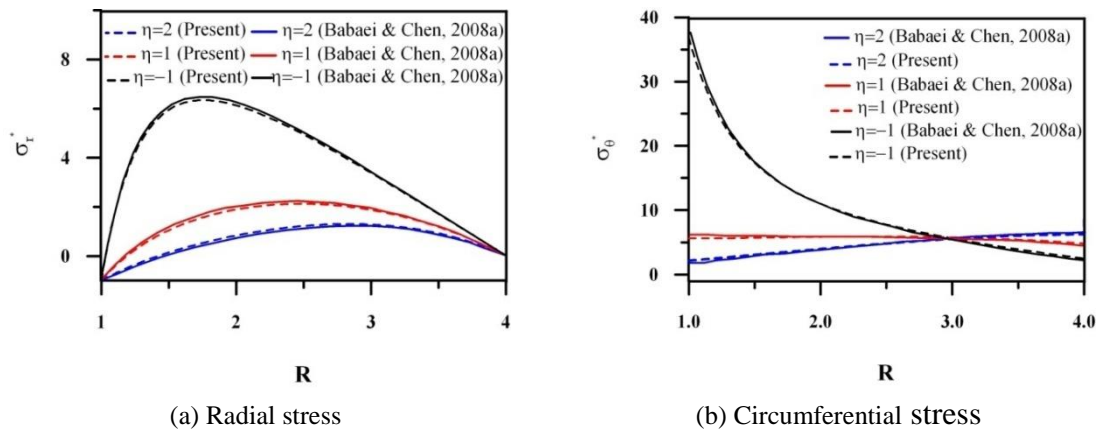


Fig. 11 Radial and circumferential stresses in rotating FGPM Hollow cylinder ( $b=4a$ )

#### 4. Conclusions

An analytical solution for the electro-magneto-thermo-elastic behavior of a rotating long hollow FGM cylinder imperfectly bonded with FGPM layers on the Winkler elastic foundation is obtained. A linear spring model is adopted to describe the weakness of the imperfect interface. All material properties except the Poisson ratio are assumed as a power function of radius. The results are of great interest due to that the effects of different parameters on the response of the hybrid cylinder can be analytically characterized using the obtained mathematical formulations. Based on the numerical value of the solution to the problem the following conclusions can be obtained.

- The radial Stress and displacement in FGM layer can be controlled more effectively by using functionally graded piezoelectric material with suitable gradient index.
- The hoop stress in the inner surface of the FGM layer significantly decreases by the use of a proper gradient index,  $\eta$ .
- Completely different static behavior of hybrid cylinder can be obtained by considering a proper gradient index ( $\eta$ ) and imposing a suitable magnetic field. The application of a proper magnetic field can reduce the hoop stress (radial stress) in a rotating hybrid cylinder and results in a more reliable hybrid structure.
- Raising the temperature on the inner surface increases the hoop stress and displacement in the hybrid cylinder. Also, there exists a fixed point at which the radial stress does not change with changing the inner temperature.
- The inner FGPM layer is more suitable than the outer FGPM layer when it is considered as an actuator. The displacement and circumferential stress are decreasing with increasing of the applied voltage in the inner FGPM layer.
- An increase of the foundation stiffness results in an increase in the absolute value of the through thickness radial stresses and a decrease in the hoop stress and displacement of the outer surface.
- The actuation authority and sensory potential of the FGPM layers is severely affected by the presence of bonding imperfections.
- It is concluded that by applying an appropriate combination of thermo-electro-magneto-mechanical boundary conditions over a rotating hybrid FG hollow cylinder, an even distribution of hoop stress can be achieved, which is valuable for designing smart structures.

#### References

- Aghaie khafri, M. and Saadatfar, M. (2013), "Analytical solution For thermo-electro-elastic stress In FGM Hollow Cylinder With Functionally graded piezoelectric layers", *Proceeding of the 21st Annual International Conference on Mechanical Engineering*, Tehran, Iran, May.
- Akbarzadeh, A.H. and Chen, Z.T. (2013), "Hygrothermal stresses in one-dimensional functionally graded piezoelectric media in constant magnetic field", *Compos. Struct.*, **97**, 317-331.
- Akbarzadeh, A.H. and Chen, Z.T. (2012), "Magneto-electroelastic behavior of rotating cylinders resting on an elastic foundation under hygrothermal loading", *Smart Mater. Struct.*, **21**(12), 125013.
- Akbarzadeh, A.H., Babaei, M.H. and Chen, Z.T. (2011), "The thermoelectromagnetoelastic behavior of a rotating functionally graded piezoelectric cylinder", *Smart Mater. Struct.*, **20**(6), 065008.
- Alibeigloo, A. and Nouri, V. (2010), "Static analysis of functionally graded cylindrical shell with piezoelectric layers using differential quadrature method", *Compos. Struct.*, **92**(8), 1775-1785.

- Alibeigloo, A., Kani, A.M. and Pashaei, M.H. (2012), "Elasticity solution for the free vibration analysis of functionally graded cylindrical shell bonded to thin piezoelectric layers", *Int. J. Pres. Ves. Piping*, **89**, 98-111.
- Alibeigloo, A. (2008), "Static analysis of an anisotropic laminated cylindrical shell with piezoelectric layers using differential quadrature method", *J. Mech. Eng. Sci.*, **222**(6), 865-880.
- Alibeigloo, A. (2011), "Thermoelastic solution for static deformations of functionally graded cylindrical shell bonded to thin piezoelectric layers", *Compos. Struct.*, **93**(2), 961-972.
- Babaei, M.H. and Chen, Z.T. (2008a), "Analytical solution for electromechanical behavior of a rotating functionally graded piezoelectric hollow shaft", *Arch. Appl. Mech.*, **78**(7), 489-500.
- Babaei, M.H. and Chen, Z.T. (2008b), "Exact solutions for radially polarized and magnetized magnetoelastothermoelastic rotating cylinders", *Smart Mater. Struct.*, **17**(2), 025-035.
- Chang, C.I. (1975), "The anisotropic rotating disks", *Int. J. Mech. Sci.*, **17**(6), 397-402.
- Chen, J.Y., Ding, H.J. and Chen, W.Q. (2007), "Three-dimensional analytical solution for a rotating disc of functionally graded materials with transverse isotropy", *Arch. Appl. Mech.*, **77**(4), 241-251.
- Chen, W.Q. and Lee, K.Y. (2004), "Exact solution of angle-ply piezoelectric laminates in cylindrical bending with interfacial imperfections", *Compos. Struct.*, **65**(3-4), 329-337.
- Chen, W.Q., Cai, J.B., Ye, J.R. and Wang, Y.F. (2004), "Exact three-dimensional solutions of laminated orthotropic piezoelectric rectangular plates featuring interlaminar bonding imperfections modeled by a general spring layer", *Int. J. Solids Struct.*, **41**(18-19), 5247-5263.
- Chen, W.Q. and Lee, K.Y. (2005), "Benchmark solution of angle-ply piezoelectric-laminated cylindrical panels in cylindrical bending with weak interfaces", *Arch. Appl. Mech.*, **74**(7), 466-476.
- Dai, H.L., Fu, Y.M. and Dong, Z.M. (2006), "Exact solutions for functionally graded pressure vessels in a uniform magnetic field", *Int. J. Solids Struct.*, **43**, 5570-5580.
- Dai, H.L. and Fu Y.M. (2007), "Magnetoelastothermoelastic interactions in hollow structures of functionally graded material subjected to mechanical loads", *Int. J. Pres. Ves. Piping*, **84**(3), 132-138.
- Dai, H.L., Fu, Y.M. and Yang, J.H. (2007) "Electromagnetoelastothermoelastic solutions for functionally graded piezoelectric solid cylinder and sphere", *Acta Mech. Sinica*, **23**, 55-63.
- Dai, H.L., Hong, L., Fu, Y.M. and Xiao, X. (2010), "Analytical solution for electro-magneto-thermo-elastic behaviors of a functionally graded piezoelectric hollow cylinder", *Appl. Math. Model.*, **34**, 343-357.
- Dai, H.L., Yang, L. and Zheng, H.Y. (2011a), "Magnetoelastothermoelastic analysis of functionally graded hollow spherical structures under thermal and mechanical loads", *Solid State Sci.*, **13**(2), 372-378.
- Dai, H.L., Rao, Y.N. and Jiang, H.J. (2011b), "An analytical method for magnetoelastothermoelastic analysis of functionally graded hollow cylinders", *Appl. Math. Comput.*, **218**(4), 1467-1477.
- Dai, H.L., Dai, T. and Zheng, Z.Y. (2012), "Stresses distributions in a rotating functionally graded piezoelectric hollow cylinder", *Meccanica*, **47**(2), 423-436.
- El-Naggar, A.M., Abd-Alla, A.M., Fahmy, A.M. and Ahmed, S.M. (2002) "Thermal stresses in a rotating non-homogeneous orthotropic hollow cylinder", *Heat Mass Transfer*, **39**(1), 41-46.
- Eraslan, A.N. and Akis, T. (2006), "On the plane strain and plane stress solutions of functionally graded rotating solid shaft and solid disk problems", *Acta Mech.*, **181**(1-2), 43-63.
- Galic, D. and Horgan, C.O. (2003), "The stress response of radially polarized rotating piezoelectric cylinders", *J. Appl. Mech.- ASME*, **70**(3), 426-435.
- Genta, G. and Gola, M. (1981), "The stress distribution in orthotropic rotating disks", *J. Appl. Mech.- ASME*, **48**(3), 559-562.
- Ghorbanpour Arani, A., Kolahchi, R. and Mosallaie Barzoki, A.A. (2011), "Effect of material in-homogeneity on electro-thermo-mechanical behaviors of functionally graded piezoelectric rotating shaft", *Appl. Math. Model.*, **35**(6), 2771-2789.
- Horgan, C.O. and Chan, A.M. (1990), "The stress response of functionally graded isotropic linearly elastic rotating disks", *J. Elast.*, **55**(3), 219-230.
- Jabbari, M., Sohrabpour, S. and Eslami, M.R. (2002), "Mechanical and thermal stresses in a functionally graded hollow cylinder due to radially symmetric loads", *Int. J. Pres. Ves. Piping*, **79**(7), 493-497.

- Javanbakht, M., Shakeri, M. and Sadeghi, S.N. (2009), "Dynamic analysis of functionally graded shell with piezoelectric layers based on elasticity", *Proc. IMechE Part C: J. Mech. Eng. Sci.*, **223**(9), 2039-2047.
- Kapuria, S. and Nair, P.G. (2010), "Exact three-dimensional piezothermoelasticity solution for dynamics of rectangular cross-ply hybrid plates featuring interlaminar bonding imperfections", *Compos. Sci. Tech.*, **70**(5), 752-762.
- Kiani, Y., Akbarzadeh, A.H., Chen, Z.T. and Eslami, M.R. (2012), "Static and dynamic analysis of an FGM doubly curved panel resting on the Pasternak-type elastic foundation", *Compos. Struct.*, **94**(8), 2474-2484.
- Kong, T., Li, D.X. and Wang, X. (2009), "Thermo-magneto-dynamic stresses and perturbation of magnetic field vector in a non-homogeneous hollow cylinder", *Appl. Math. Model.*, **33**(7), 2939-2950.
- Li, Y.D. and Lee, K.Y. (2009), "Crack tip shielding and anti-shielding effects of the imperfect interface in a layered piezoelectric sensor", *Int. J. Solids Struct.*, **46**, 1736-1742.
- Reddy, T.Y. and Srinath, H. (1974), "Elastic stresses in a rotating anisotropic annular disk of variable thickness and variable density", *Int. J. Mech. Sci.*, **16**(2), 85-89.
- Saadatfar, M. and Razavi, S.A. (2009), "Piezoelectric hollow cylinder with thermal gradient", *J. Mech. Sci. Tech.*, **23**, 47-55.
- Shakeri, M., Sadeghi, S.N. and Javanbakht, M. (2009), "Dynamic analysis of functionally graded plate integrated with two piezoelectric layers, based on a three-dimensional elasticity solution", *Proc. IMechE Part C: J. Mech. Eng. Sci.*, **223**(6), 1297-1309.
- Shen, H.S. and Noda, N. (2007), "Postbuckling of pressure-loaded FGM hybrid cylindrical shells in thermal environments", *Compos. Struct.*, **77**, 546-560.
- Tutuncu, N. (2007), "Effect of anisotropy on stresses in rotating discs", *Int. J. Mech. Sci.*, **37**(8), 873-881.
- Wang, H.M., Ding, H.J. and Ge, W. (2007), "Transient responses in a two-layered elasto-piezoelectric composite hollow cylinder", *Compos. Struct.*, **79**(2), 192-201.
- Wang, H.M. (2011), "Dynamic electromechanical behavior of a triple-layer piezoelectric composite cylinder with imperfect interfaces", *Appl. Math. Model.*, **35**, 1765-1781.
- Wang, H.M. (2010), "Effect of material inhomogeneity on the rotating functionally of a graded orthotropic hollow cylinder", *J. Mech. Sci. Tech.*, **24**(9), 1839-1844.
- Wang, X. and Dong, K. (2006), "Magnetothermodynamic stress and perturbation of magnetic field vector in a non-homogeneous thermoelastic cylinder", *Eur. J. Mech. A/Solids*, **25**, 98-109.
- Xiang, H.J. and Shi, Z.F. (2009), "Static analysis for functionally graded piezoelectric actuators or sensors under a combined electro-thermal load", *Eur. J. Mech. A/Solids*, **28**(2), 338-346.
- Yas, M.H., Shakeri, M. and Khanjani, M. (2011), "Layer-wise finite-element analysis of a functionally graded hollow thick cylinder with a piezoelectric ring", *Proc. IMechE Part C: J. Mech. Eng. Sci.*, **225**(5), 1045-1060.
- Ying, J., Lu, C.F. and Chen, W.Q. (2008), "Two-dimensional elasticity solutions of functionally graded beams resting on elastic foundations", *Compos. Struct.*, **84**(3), 209-19.

## Appendix

In this section, components of matrixes X and F are given for a FGME hollow sphere. According to mechanical boundary conditions (43.a), we obtain

$$X = [X_1 X_2 \dots X_{10}] \quad (\text{A.1})$$

$$X_1 = [(C_1 m_1 + C_2) a^{\beta+m_1-1} \ 0 \ (C_4 + \frac{C_7}{m_1}) a^{m_1} \ (C_4 + \frac{C_7}{m_1}) b^{m_1} \ 0 \ 0 \ (C_1 m_1 + C_2) b^{\beta+m_1-1} \ 0 \ -b^{m_1} \ 0]^T$$

$$X_2 = [(C_1 m_2 + C_2) a^{\beta+m_2-1} \ 0 \ (C_4 + \frac{C_7}{m_2}) a^{m_2} \ (C_4 + \frac{C_7}{m_2}) b^{m_2} \ 0 \ 0 \ (C_1 m_2 + C_2) b^{\beta+m_2-1} \ 0 \ -b^{m_2} \ 0]^T$$

$$X_3 = [(\frac{W_6}{W_1}(C_2 - \beta C_1) - C_4) a^{-1} \ 0 \ (\frac{W_6}{W_1}(C_4 - \frac{C_7}{\beta}) - \frac{1}{g_{11}^0 \beta}) a^{-\beta} \ (\frac{W_6}{W_1}(C_4 - \frac{C_7}{\beta}) - \frac{1}{g_{11}^0 \beta}) b^{-\beta} \\ 0 \ 0 \ (\frac{W_6}{W_1}(C_2 - \beta C_1) - C_4) b^{-1} \ 0 \ -\frac{W_6}{W_1} b^{-\beta} \ 0]^T$$

$$X_4 = [0 \ 0 \ 1 \ 1 \ 0 \ 0 \ 0 \ 0 \ 0 \ 0]^T$$

$$X_5 = [0 \ 0 \ 0 \ 0 \ 0 \ 0 \ -\frac{E_0((1-\nu)\eta_1 + \nu)}{(1+\nu)(1-2\nu)} b^{\eta+\eta_1-1} \ -\frac{E_0((1-\nu)\eta_1 + \nu)}{(1+\nu)(1-2\nu)} c^{\eta+\eta_1-1} \\ b^{\eta_1} - \frac{\zeta_1 E_0((1-\nu)\eta_1 + \nu)}{(1+\nu)(1-2\nu)} b^{\eta+\eta_1-1} \ -c^{\eta_1} + \frac{\zeta_2 E_0((1-\nu)\eta_1 + \nu)}{(1+\nu)(1-2\nu)} c^{\eta+\eta_1-1}]^T$$

$$X_6 = [0 \ 0 \ 0 \ 0 \ 0 \ 0 \ -\frac{E_0((1-\nu)\eta_2 + \nu)}{(1+\nu)(1-2\nu)} b^{\eta+\eta_2-1} \ -\frac{E_0((1-\nu)\eta_2 + \nu)}{(1+\nu)(1-2\nu)} c^{\eta+\eta_2-1} \\ b^{\eta_2} - \frac{\zeta_1 E_0((1-\nu)\eta_2 + \nu)}{(1+\nu)(1-2\nu)} b^{\eta+\eta_2-1} \ -c^{\eta_2} + \frac{\zeta_2 E_0((1-\nu)\eta_2 + \nu)}{(1+\nu)(1-2\nu)} c^{\eta+\eta_2-1}]^T$$

$$X_7 = [0 \ (C'_1 m'_1 + C'_2) d^{\beta+m'_1-1} \ 0 \ 0 \ (C'_4 + \frac{C'_7}{m'_1}) c^{m'_1} \ (C'_4 + \frac{C'_7}{m'_1}) d^{m'_1} \ 0 \ (C'_1 m'_1 + C'_2) c^{\beta+m'_1-1} \ 0 \ c^{m'_1}]^T$$

$$X_8 = [0 \ (C'_1 m'_2 + C'_2) d^{\beta+m'_2-1} \ 0 \ 0 \ (C'_4 + \frac{C'_7}{m'_2}) c^{m'_2} \ (C'_4 + \frac{C'_7}{m'_2}) d^{m'_2} \ 0 \ (C'_1 m'_2 + C'_2) c^{\beta+m'_2-1} \ 0 \ c^{m'_2}]^T$$

$$X_9 = \left[ 0 \left( \frac{W'_6}{W'_1} (C'_2 - \beta C'_1) - C'_4 \right) d^{-1} \quad 0 \quad 0 \quad \left( \frac{W'_6}{W'_1} (C'_4 - \frac{C'_7}{\beta}) - \frac{1}{g_{11}^{0'} \beta} \right) c^{-\beta} \quad \left( \frac{W'_6}{W'_1} (C'_4 - \frac{C'_7}{\beta}) - \frac{1}{g_{11}^{0'} \beta} \right) d^{-\beta} \right. \\ \left. 0 \left( \frac{W'_6}{W'_1} (C'_2 - \beta C'_1) - C'_4 \right) c^{-1} \quad 0 \quad \frac{W'_6}{W'_1} c^{-\beta} \right]^T$$

$$X_{10} = [0 \ 0 \ 0 \ 0 \ 1 \ 1 \ 0 \ 0 \ 0 \ 0]^T$$

$$F = F_2 - F_1$$

$$F_1 = [S_1(r=a) \ S'_1(r=d) \ S_2(r=a) \ S_2(r=b) \ S'_2(r=c) \ S'_2(r=d) \\ S_3(r=b) \ S'_3(r=c) \ S_4 \ S_5]^T$$

$$F_2 = [-P_i \ -P_o \ \phi_a \ \phi_b \ \phi_c \ \phi_d \ 0000]^T$$

$$S_1 = C_2(B_3 r^\beta + B_4 r^{2\beta} + B_5 + B_6 r^{2+\beta}) + (C_3 - \lambda_1^0 r^\beta)(w_1^i + w_2^i r^\beta) \\ C_1(B_3 r^\beta + B_4(\beta+1)r^{2\beta} + B_5(-\beta+1) + 3B_6 r^{2+\beta})$$

$$S_2 = (C_4 + C_7)B_3 r + (C_4 + \frac{C_7}{\beta+1})B_4 r^{\beta+1} + (C_4 + \frac{C_7}{-\beta+1})B_5 r^{-\beta+1} + (C_4 + \frac{C_7}{3})B_6 r^3 \\ + \frac{P_{11}^0}{g_{11}^0} \left( \frac{w_1^i}{-\beta+1} r^{-\beta+1} + w_2^i r \right)$$

$$S_3 = C_2(B_3 r^\beta + B_4 r^{2\beta} + B_5 + B_6 r^{2+\beta}) + (C_3 - \lambda_1^0 r^\beta)(w_1^i + w_2^i r^\beta) \\ + C_1(B_3 r^\beta + B_4(\beta+1)r^{2\beta} + B_5(-\beta+1) + 3B_6 r^{2+\beta}) - \frac{E_0}{(1+\nu)(1-2\nu)} [(D_3 - (1+\nu)\alpha_0 w_3) r^\eta \\ + ((\eta - \nu\eta + 1)D_4 - (1+\nu)\alpha_0 w_4) r^{2\eta} + D_5(3-2\nu)r^{2+\eta}]$$

$$S_4 = (-B_3 b \ -B_4 b^{\beta+1} - B_5 b^{-\beta+1} - B_6 b^3 + D_3 b + D_4 b^{\eta+1} + D_5 b^3) \\ + \frac{\zeta_1 E_0}{(1+\nu)(1-2\nu)} [(D_3 - (1+\nu)\alpha_0 w_3) b^\eta + ((\eta - \nu\eta + 1)D_4 - (1+\nu)\alpha_0 w_4) b^{2\eta} + D_5(3-2\nu)b^{2+\eta}]$$

$$S_5 = (B'_3 c \ +B'_4 c^{\beta+1} + B'_5 c^{-\beta+1} + B'_6 c^3 - D_3 c - D_4 c^{\eta+1} - D_5 c^3) \\ + \frac{\zeta_1 E_0}{(1+\nu)(1-2\nu)} [(D_3 - (1+\nu)\alpha_0 w_3) c^\eta + ((\eta - \nu\eta + 1)D_4 - (1+\nu)\alpha_0 w_4) c^{2\eta} + D_5(3-2\nu)c^{2+\eta}]$$

where parameters with prime symbol ( ' ) is used to represent the corresponding value for the outer FGPM layer. For mechanical boundary conditions (43.b), the following components of matrixes in Eq. (A.1) are modified as

$$\begin{aligned}
 X_1(1,1) &= -K_w a^{m_1} + (C_1 m_1 + C_2) a^{\beta+m_1-1} \\
 X_2(1,1) &= -K_w a^{m_2} + (C_1 m_2 + C_2) a^{\beta+m_2-1} \\
 X_3(1,1) &= \left( \frac{W_6}{W_1} (C_2 - \beta C_1 - K_w a^{-\beta+1}) - C_4 \right) a^{-1} \\
 F_1(1,1) &= S_1(r=a) - K_w (B_3 a + B_4 a^{\beta+1} + B_5 a^{-\beta+1} + B_6 a^3) \\
 F_2(1,1) &= 0
 \end{aligned} \tag{A.2}$$

For mechanical boundary conditions (43.c), following components of matrixes in Eq. (A.1) are modified

$$\begin{aligned}
 X_7(2,1) &= K_w d^{m'_1} + (C'_1 m'_1 + C'_2) d^{\beta+m'_1-1} \\
 X_8(2,1) &= K_w d^{m'_2} + (C'_1 m'_2 + C'_2) d^{\beta+m'_2-1} \\
 X_9(2,1) &= \left( \frac{W_6}{W_1} (C'_2 - \beta C'_1 + K_w d^{-\beta+1}) - C'_4 \right) d^{-1} \\
 F_1(2,1) &= S'_1(r=d) + K_w (B'_3 d + B'_4 d^{\beta+1} + B'_5 d^{-\beta+1} + B'_6 d^3) \\
 F_2(2,1) &= 0
 \end{aligned} \tag{A.3}$$

Besides, for mechanical boundary conditions (43.d), both of modified components that defined in Eqs. (A.3) and (A.4) should be used.